Springer

KSME

Journal of Mechanical Science and Technology 24 (2010) 73~76
www.springerlink.com/content/1738-494x
DOI 10.1007/s12206-009-1115-8

Estimations of work hardening exponents of engineering metals using residual indentation profiles of nano-indentation †

Byung-Min Kim[1], Chan-Joo Lee[2] and Jung-Min Lee[2,*]

[1]*School of Mechanical Engineering, Pusan National University, Busan, Korea*
[2]*Dept. of Precision Manufacturing Systems Engineering, Pusan National Univ., Busan, Korea*

(Manuscript Received May 4, 2009; Revised September 30, 2009; Accepted October 12, 2009)

Abstract

This study was designed to predict work hardening exponent *n* of materials from AFM (atomic force microscope) observations of residual indentation impression in sharp indentations. FE simulations of nano-indentation were performed to 140 combinations to each parameter (elastic modulus *E*, yield stress σ_y, work hardening exponent *n*, and Poisson's ratio ν) expressing elastic-plastic behaviors of universal engineering metals. Using the results from FE simulations and dimensional analysis, dimensionless functions were established to correlate residual indentation profiles with the work hardening exponent. This function was examined with nano-indentation, tensile test, and AFM observations after indentation for two materials (Al6061-T6 and copper).

Keywords: Nano-indentation; Work hardening exponent; AFM observation; Engineering metal

1. Introduction

One of the main features of nano-indentation technique is the indirect measurement of the contact area between the indenter and materials during indentation. However, the formation of pile-up and sink-in in contact during indentation involves either an overestimation or underestimation of the true contact area [1]. Fischer-Cripps [1, 2] reported that the real contact area of the indenter could be underestimated up to 60% for a certain material in a pile-up, thereby leading to the overestimation of elastic modulus *E* and hardness. In general, for engineering metals, including elastic-plastic deformations, behaviors of pile-up and sink-in are mainly dependent on their E/σ_y and the work hardening exponent *n* [1-3].

This paper was designed to estimate *n* of the engineering metals from AFM observations of residual indentation impression in nano-indentation using a sharp indenter. FE simulations of a sharp indentation were performed to 140 different combinations of elastic-plastic parameters (E, σ_y, n, ν), which represent the power-law behavior of typical engineering metals. Using simulated results and the dimensional analysis, the dimensionless function was constructed to relate the residual indentation profile to *n* of the indented material. Finally, the constructed function was examined with nano-indentation, tensile tests, and AFM observations for the two materials (Al6061-T6 and copper).

2. FE simulations of indentation and dimensional analysis

FE simulations of nano-indentation and dimensional analysis were based on Lee and Dao's studies [4, 5]. The power law true-stress/true-strain curve of the engineering metals in the uniaxial tensile state (Fig. 1) can be assumed as [1, 4, 5]

$$\sigma = E\varepsilon \text{, for } \varepsilon \le \frac{\sigma_y}{E} \text{ and } \sigma = K\varepsilon^n \text{, for } \varepsilon \ge \frac{\sigma_y}{E} \qquad (1)$$

where *K* is strength coefficient. The continuity of the curve in Eq. (1) requires $K = \sigma_y (E/\sigma_y)^n$. Therefore, E, n, σ_y, and ν are independent parameters describing the power law behavior of the material. Applying reduced modulus E^* and

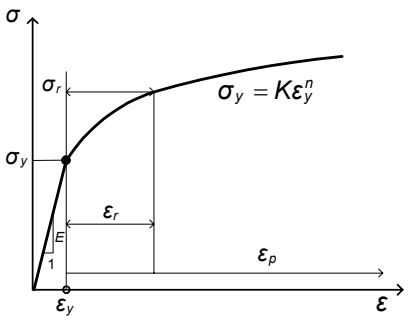

Fig. 1. The power law elastic-plastic stress-strain behavior of metals.

† This paper was presented at the ICMDT 2009, Jeju, Korea, June 2009. This paper was recommended for publication in revised form by Guest Editors Sung-Lim Ko, Keiichi Watanuki.

*Corresponding author. Tel.: +82 51 510 3074, Fax.: +82 51 581 3075
E-mail address: monkey1976@pusan.ac.kr

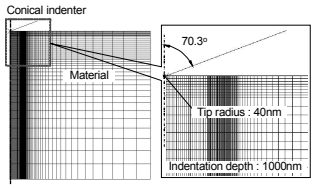

Fig. 2. FE model of sharp nanoindentation (70.3°).

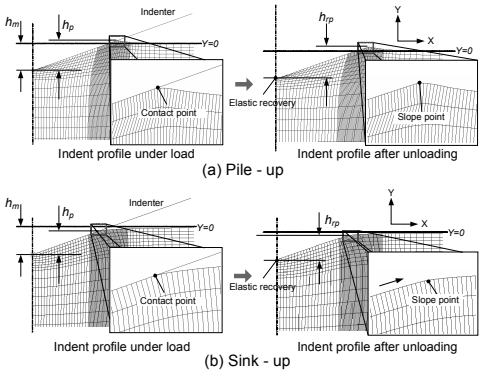

Fig. 3. Definitions of the contact boundary of pile-up and sink-in under full load and after complete unloading.

representative stress σ_r [5], instead of E and σ_y, the behavior is represented as E^*, σ_r, ν, and n [4-6].

FE simulations were carried out for to a total of 140 cases: E varied from 10 to 600 GPa, σ_y from 10 to 2500 MPa, and n from 0.01 to 0.5 at 0.1 intervals, and ν was fixed at 0.3. For both the Berkovich and Vickers indenters ($A = 24.56h_m^2$), the corresponding apex angle of their two dimensional cones is 70.3°. [1] The FE model of nano-indentation (Fig. 2) was assumed to be axisymmetric and two-dimensional, and the indenter was modeled as a rigid body. The contact between the indenter and materials was assumed to be frictionless [7]. The maximum indentation depth h_m was 1000nm, where by which the size effect of the indented material was negligible [5]. All the simulations were performed using ABAQUS 6.3-1.

Fig. 3 shows the definitions of the contact boundary of pile-up and sink-in under full load and after complete unloading for FE simulations of the 140 cases. This study used h_p / h_m and h_{rp} / h_m were used as independent parameters to estimate the amount of pile-up and sink-in before and after indentation. Here, h_p and h_{rp} are the indentation depths by pile-up and sink-in under full load and after unloading, respectively. Using the dimensional analysis, the degree of pile-up and sink-in is expressed as:

$$\frac{h_p}{h_m} = \Pi_1\left(\frac{E^*}{\sigma_r}, n\right) \quad \text{at } h_m \text{ during loading} \tag{2}$$

and

$$\frac{h_{rp}}{h_m} = \Pi_2\left(\frac{E^*}{\sigma_r}, n\right) \quad \text{after unloading} \tag{3}$$

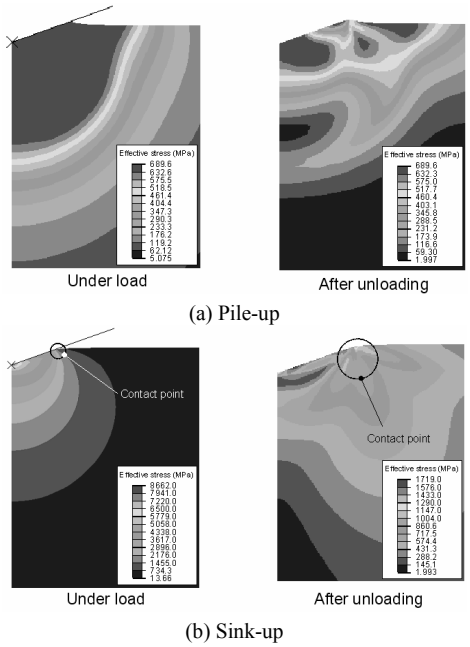

Fig. 4. Effective stress distributions beneath the indenter for piled-up and sank-in materials under load and after unload.

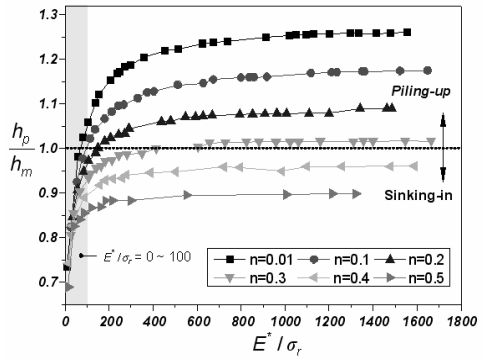

Fig. 5. Effects of different E^* / σ_r and n values on the degree of pile-up/sink-in h_p / h_m under load.

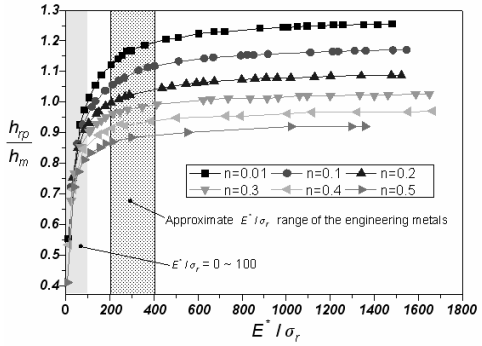

Fig. 6. Effects of different E^* / σ_r and n values on the degree of pile-up/sink-in h_{rp} / h_m after complete loading.

3. Results and experiments

3.1 Results of FE simulations

Fig. 4 shows the stress distributions of materials beneath the

indenter for pile-up (E= 500GPa, σ_y = 150MPa, n= 0.5) and sink-in (E= 240GPa, σ_y = 650MPa, n= 0.01) at full load and after complete unloading. In the case of pile-up, the maximum stress distributions under load were observed to have a hemispherical shape and located widely over the piled -up part. Also, the residual stress distributions after unloading were extensively placed near the indenter and the piled -up part. In the case of sink-in, the stress distributions beneath the indenter were limited within the contact radius and were more deeply formed compared to those in the pile-up. Also, the maximum stress distributions were concentrated near the indenter tip. However, the residual stress distributions after unloading were concentrated at the sink-in part, and the values were also very low in terms of elastic recovery. For sink-in, the amount of elastic recovery and the difference between stress values at loading and after unloading were much larger than those in the pile-up [1, 2].

The E^*/σ_r values for each material of the 140 cases in FE simulations were determined from Lee's study [4]. Fig. 5 shows h_p/h_m with different n values under full load. Indentation profiles were divided according to pile-up and sink-in at approximately n = 0.3. In general, the pile-up and sink-in of the indented material were very much dependent on their n values at around $400 < E^*/\sigma_r$. However, they depended heavily on E^*/σ_r, not n, at about $400 > E^*/\sigma_r$. Also, the only sink-in was dominant, especially at about $100 > E^*/\sigma_r$, indicating properties like polymeric materials with high elastic strain. Fig. 6 shows h_{rp}/h_m with different n values after complete unloading. Since h_{rp} of pile-up may be smaller than h_m due to high elastic recovery of the indenter's apex, it is difficult to distinguish scenarios of pile-up/sink-in from Fig. 5. However, n of the indented materials can be characterized by their residual indentation depth using these data. Therefore, the dimensionless Π_2 function to determine n of the indented material after complete unloading can be given by Eq. (3) and its closed form are shown to be completed by fitting all 140 data points within ±3.0% errors in Fig. 6 (Appendix A).

3.2 Experiments

To verify the validity of the dimensionless Π_2 function (Appendix A), nano-indentation and uniaxial tensile tests were performed for Al6061-T6 and copper (99%), whose typical n values were roughly 0.1 and 0.4, respectively. Thus, the materials cwould provide the obvious pile-up and sink-in during nano-indentation. Indentation specimens were machined from the same round bar stock as discs of the bar diameter (10 mm thickness). Each specimen was polished to average surface roughness R_a of 3 ~ 17nm. These specimens were indented on a commercial Nanoindenter XP of MTS with the Berkovich diamond indenter up to an indentation depth of 1000 nm at a target strain rate of approximately 0.05. Nano-indentation tests were repeatedly conducted nine times for each material. AFM observations after indentation were performed using the commercial XE-100 of Park Systems.

Table 1. Results of uniaxial tensile test for each material.

	E(GPa)	σ_y (MPa)	n
Al6061-T6	70.6	331.7	0.081
Copper	110	35.7	0.456

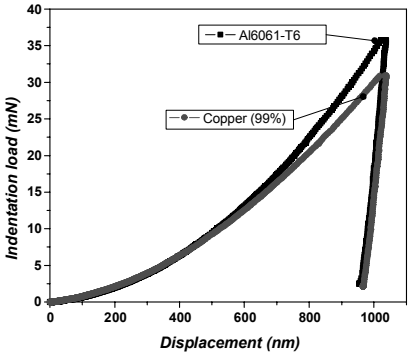

Fig. 7. Load - displacement curves of Al6061-T6 and copper (99%).

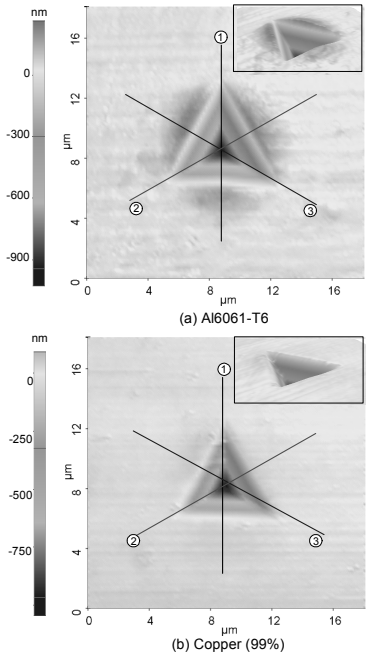

Fig. 8. AFM observations of Al6061-T6 and copper after indentation.

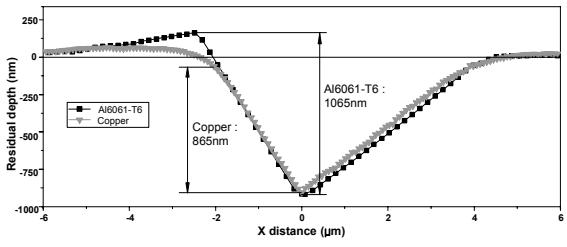

Fig. 9. Residual indentation profiles of Al6061-T6 and copper all 140 data points within ± 3.0% errors in Fig. 6 (Appendix A).

For each material, results of nano-indentation and tensile tests (E, σ_y (0% offset) and n) are shown in Fig. 7 and Table

Table 2. E^*/σ_r and h_p/h_m of each materials and the estimated n from Π_2 functions.

	E^*/σ_r	hrp/hm	n (Π_2 function)
Al6061-T6	191.17	1.065	0.075
Copper	110	0.865	0.466

1, respectively. Fig. 8 shows the typical AFM images of the residual indentation impressions after indentation of the two materials, which showed scenarios of obvious pile-up for Al6061-T6 with n=0.081 and sink-in for copper with n=0.456. Fig. 9 shows the residual indentation profiles of two materials, which are the average profiles measured for three locations marked in Fig. 8.

3.3 Estimations of work hardening exponents

Detailed procedure to obtain E^*/σ_r of Al6061-T6 and copper used in this study was referred in Lee's work [ ]. Also, h_{rp} values of each material after indentation were obtained from Fig. 9. E^*/σ_r and h_{rp}/h_m of Al6061-T6, as well as the copper used to estimate n and the subsequently calculated n values using the Π_2 function are listed in Table 2.

The Π_2 functions provide relatively accurate estimates of n with -8.0% errors for Al6061-T6 and with 9.19% errors for copper (99%) compared to the tensile tests. These errors are due to the difference between each of the pile-up/sink-in generated by Berkovich and its equivalent cone indenters. The Π_2 function was established based on the equivalent cone indenter. Therefore, the entire amounts of pile-up and sink-in obtained from AFM observations (Fig. 9) and the further extracted n could be somewhat overestimated in the case of the Berkovich indenter. To calibrate differences, the definition of geometric relation between each pile-up and sink-in created by two indenters is required. We will discuss the problem in future research. Consequently, Π_2 function can be used as a simple method for estimating the approximate n from the residual indentation impression of nano-indentation.

4. Conclusions

This study was performed to relate residual indentation profile to the work hardening exponent of the indented material. The residual indentation profiles of the indented material were divided into scenarios of pile-up and sink-in at approximately n= 0.3. Also, the phenomena of pile-up and sink-in were dependent on E^*/σ_r, as well as n at around $200 < E^*/\sigma_r < 400$, which is the approximate range of the engineering metals. From this relation, the dimensionless Π_2 function was set up to relate the work hardening exponent and residual indentation profile of the indented material. The n values extracted from the function agreed well with those of the tensile tests within ±10% errors.

Acknowledgments

This work was supported by KICOS through a grant provided by MEST in 2008 (No. K2060111114-08E0100-00410) and a grant-in-aid for the NCRC Program of MOST and KOSEF (No. R15-2006-022-03003-0).

References

[1] A. C. Fischer-Cripps, *Nanoindentation*, Springer-Verlag, New York, USA, (2002).

[2] A. C. Fischer-Cripps, A review of analysis methods for sub-micron indentation testing, *Vacuum*, 58 (2000) 569-585.

[3] A. Bolshakov and G. M. Pharr, Influence of piling-up on the measurement of mechanical properties by load and depth sensing indentation techniques, *Journal of material research*, 13 (4) (1998) 1049-1058.

[4] J. M. Lee et al., Improvement of Dao's reverse analysis and determination of representative strain for extracting elastic-plastic properties of materials in analysis of nanoindentation, *Journal of KSME-A*, 32 (2) (2008) 105-118.

[5] M. Dao et al., Computational modeling of the forward and reverse problems in instrumented sharp indentation, *Acta materialia*, 49 (2001) 3899-3918.

[6] Y. T. Cheng and C. M. Cheng, Scaling, dimensional, and indentation measurements, *Material science and Engineering R* 44 (2004) 91-149.

[7] J. L. Bucaille et al., Determination of plastic properties of metals by instrumented indentation using different sharp indenters, *Acta materialia*, 51 (2003) 1663-1678.

Byung-Min Kim received his B.S. degree (1979), M.S. (1984) and Ph.D. (1987) from Pusan National University. He is currently a Professor at the School of Mechanical Engineer-ing at Pusan National University, and currently serving as a Director in PNU-IFAM Joint Research Center. His major area is metal forming process and hybrid joining technology.

Jung-Min Lee received his B.S. Degree(2001), M.S. (2003) and Ph.D. (2008) from Pusan National University. He is currently a Researcher at Korea Institute of Materials Science. His major area is metal forming process.

Appendix A

$$\frac{h_{rp}}{h_m} = \Pi_2\left(\frac{E^*}{\sigma_r}, n\right)$$

$$= (0.81337n^3 - 0.47142n^2 + 0.08989n - 0.0012)\left[\ln\left(\frac{E^*}{\sigma_r}\right)^3\right]$$

$$+(-13.1679n^3 + 7.56303n^2 - 1.42724n - 0.01267)\left[\ln\left(\frac{E^*}{\sigma_r}\right)^2\right]$$

$$+(69.70148n^3 - 39.6247n^2 + 7.26262n + 0.35985)\left[\ln\left(\frac{E^*}{\sigma_r}\right)\right]$$

$$+(-122.25n^3 + 69.1623n^2 - 12.6147n - 1.25403)$$